Preparation of VZrHfNbTa high-entropy alloy-based high-temperature oxidation-resistant coating and its bonding mechanism

Mengjun Hu , Rui Tan , Junyu Chen , Meilong Hu * , Yu Yang *

Posted Date: 28 June 2023

doi: 10.20944/preprints202306.1962.v1

Keywords: High-entropy alloys; oxidation; surface; principal component analysis; mechanical properties; composites

Article

Preparation of VZrHfNbTa High-Entropy Alloy-Based High-Temperature Oxidation-Resistant Coating and Its Bonding Mechanism

Hu Mengjun [1], Tan Rui [2], Chen Junyu [2], Hu Meilong [2,*] and Yang Yu [3,*]

[1] School of Mechanical Engineering and Automation, Chongqing Industry Polytechnic College, Chongqing 401120, China

[2] School of Materials Science and Engineering, Chongqing University, Chongqing 400044, China

[3] Comprehensive Testing and Analyzing Center, North China University of Science and Technology, Tangshan 063210, China

* Correspondence: **author:** Meilong Hu, Yang Yu E-mail: hml@cqu.edu.cn (M.Hu) Phone: +86-23-65112631; Fax: +86-23-65112631 Address: College of Materials Science and Engineering, Chongqing University, Chongqing 400044, China

Abstract: Ultra-high temperature oxidation-resistant alloys (UTORAs) have received a lot of attention due to the increased research demand for deep space exploration around the world. But UTORAs have the disadvantages of easy oxidation and chalking. So, in this study, a UTORA was prepared by hot-press sintering on VZrHfNbTa (HEA) substrate coated with hafnium. The bonding mechanism, resistance to high-temperature oxidation, and hardness of the sample tests were carried out. The results show that zirconium in the matrix will diffuse into the hafnium coating during the high-temperature sintering process and form the HfZr alloy transition layer, the coating thickness of the composite is about 120 μm, and the diffusion distance of zirconium in the hafnium coating is about 60 μm, this transition layer chemically combines the hafnium coating and the HEA substrate into a monolithic alloy composite. The results of high-temperature oxidation experiments show that the oxidation degree of the hafnium-coated VZrHfNbTa composite material was significantly lower than that of the VZrHfNbTa HEA after oxidation in air at 1600 °C for 5 h. The weight gain of the coated sample after oxidation is 56.56 mg/cm^2, which was only 57.7 % compared to the weight gain of the uncoated sample (98.09 mg/cm^2 for uncoated), and the surface of the uncoated HEA showed obvious dents, oxidation, and pulverization occurred on the surface and interior of the sample. In contrast, the coated composite alloy sample mainly underwent surface oxidation sintering to form a dense HfO_2 protective layer, and the internal oxidation of the hafnium-coated VZrHfNbTa composite alloy was significantly lower than that of the uncoated VZrHfNbTa HEA.

Keywords: high-entropy alloys; oxidation; surface; principal component analysis; mechanical properties; composites

1. INTRODUCTION

With the continuous exploration of extreme environments such as deep space, deep sea, and outer space, there is an increasing requirement for functional materials capable of withstanding ultra-high and ultra-low temperatures as well as corrosion resistance. High-temperature alloys are the main materials serving as core components in frontier technologies such as aerospace and nuclear industries, such as engines, gas turbines, and high-temperature structural parts. These alloys require high strength, high-temperature fatigue resistance, oxidation resistance, and thermal corrosion capability. However, high-temperature and oxidation have become the primary problems that limit the further application of high-temperature alloys in extreme environments.

Comprehensive consideration of existing high-temperature oxidation-resistant materials, the main high-temperature oxidation-resistant alloys used in engineering are iron, cobalt, and nickel-based alloys. The cost of iron-based high-temperature alloys is relatively lower, but poorer high-

 doi:10.20944/preprints202306.1962.v1

temperature stability. FeAl intermetallic compounds [1] have better temperature resistance and excellent mechanical properties than ceramic materials, but they are limited by their inherent brittleness. Cobalt-based high-temperature alloys are strengthened mainly by the precipitation of carbides and a solid solution of refractory elements [2,3]. There are also imbalances in the performance of both the results of the two strengthening methods and the results of the improved experiments [4-7]. Their high-temperature stability and mechanical properties are much lower than those of nickel-based high-temperature alloys. Nickel-based high-temperature alloys have excellent comprehensive properties and they are widely used high-temperature structural materials at present [8]. Therefore, niobium-based alloys have received attention due to the lower liquid-phase line temperature and the limitation of their melting point, but their limited service temperature [9] can no longer meet the temperature-bearing capacity required for advanced aero-engines [10]. Although niobium-based alloys have ideal high-temperature mechanical properties [11,12], they suffer from serious oxidation problems at high temperatures [13,14], for example, niobium-silicon-based alloys. The alloys currently used in industry have problems in the high-temperature oxidation environment such as pulverization and mechanical property imbalance. It has been reported [15-17] that an alloy material resistant to high-temperature oxidation has been developed by scholars internationally and it can operate at 1800-2000C°, but the material has not been found domestically. Therefore, this study aims to establish an experimental foundation for subsequent research.

In recent years, with a lot of research on High-entropy alloys(HEAs), refractory HEAs have gradually received attention due to their excellent properties. For instance, alloys such as NbMoTaW and NbMoTaWV can operate at 1600 °C although they show a decrease in performance [18], which surpassing to the working temperature of existing alloys. HEAs offer the potential to sustain materials' function properly in ultra-high temperature environments. Among all the publicly reported HEA systems, the constituent elements are mainly refractory metal elements such as titanium, zirconium, niobium, molybdenum, hafnium, tantalum, wolfram, vanadium, etc, which have higher melting points and strength, and excellent properties at higher temperatures, making them one of the most promising high-temperature structural metals [19-22]. Currently, the most effective measure to prevent HEA materials' oxidative failure is to prepare antioxidant coatings on the material surface [23]. In this paper, the preparation of HEA-based hafnium coatings and related properties was carried out by using a hot-pressure sintering process to provide some research basis for the study of high-temperature resistant composites.

2. EXPERIMENT

In this study, VZrHfNbTa HEA-based surface metal hafnium coating material was prepared by the hot-press sintering process, and the preparation method can be described as the "embedding hot-press method", as shown in Figure 1. Prepared VZrHfNbTa HEA powder (synthesized by the electro-deoxidation process) was first compressed into a cylindrical shape using a metal-chromium steel mold with a diameter of 8 mm, applying a pressure of 4 MPa. Prepared metal hafnium powder (synthesized by electro-deoxidation) was uniformly laid flat on the bottom of a cylindrical graphite mold with a diameter of 10 mm, and the powder was separated from the mold by carbon paper. Then the pressed block of VZrHfNbTa HEA was laid flat on the metal hafnium powder. Finally pressed into the indenter, the mold was hot pressed and sintered at high temperature in a hot press sintering furnace. In the hot pressing sintering process, the set temperature is 1823 K with a 10 K/min heating rate, the pressure is 30 MPa, and the holding pressure is kept for 1 h at 1823 K. After finishing, the sample is cooled to normal temperature by cooling in the furnace.

Preprints (www.preprints.org) | NOT PEER-REVIEWED | Posted: 28 June 2023 doi:10.20944/preprints202306.1962.v1

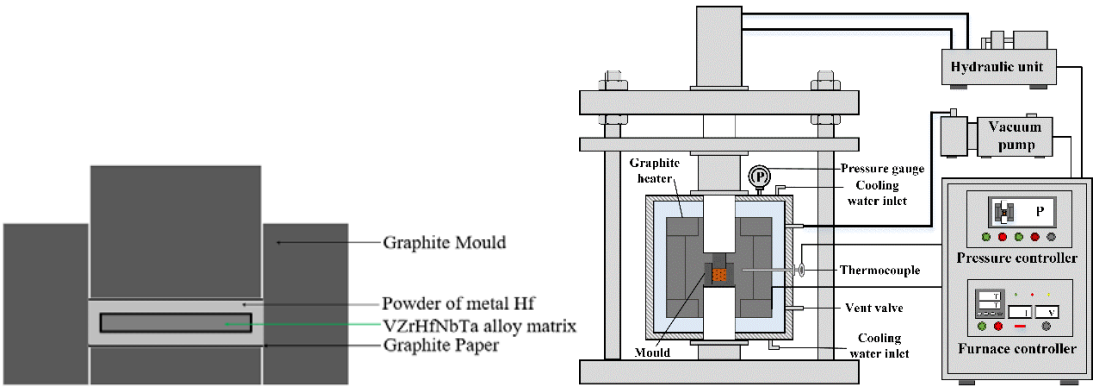

Figure 1. Schematic diagram of coating preparation by hot-press sintering process.

3. RESULTS AND DISCUSSION

Figure 2 shows the X-ray Diffraction（XRD）spectrum of the surface of the Hf-coated sample prepared by hot-press sintering. This suggests that the main phase of the surface coating is HfC, and it is easy for hafnium to react with carbon to form carbide in the carbon environment, which can increase the hardness of the coating. Based on the thermodynamic calculations of the equilibrium module in the software Factsage 8.1, the value of the Gibbs free energy for the reaction of hafnium with carbon to form an HfC solid at 1600 °C is much less than 0, which means that the reaction can proceed spontaneously at 1600 °C.

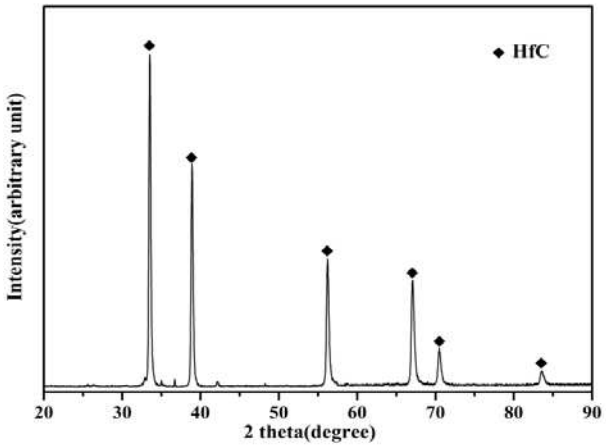

Figure 2. XRD pattern of the coating of the sample prepared by the hot-press sintering process.

Figure 3 shows the surface Scanning Electronic Microscopy（SEM）photographs of the Hf-coated samples prepared by hot-press sintering. As seen in Figure 3(a) and 3(b), there are cracks on the surface of the coating. This is due to the sintering volume shrinkage of the high melting point HfC in the coating at 1823 K. Further magnification of the area of the cracks reveals the internal sintering, as shown in Figure 3(c) and 3(d). The metal hafnium powder particles forming the coating are bonded to each other, and the diameter of small particles is less than 1 μm. The width of the cracks is less than 1 μm, which ensures the eminent density and strength of the coating.

Preprints (www.preprints.org) | NOT PEER-REVIEWED | Posted: 28 June 2023 doi:10.20944/preprints202306.1962.v1

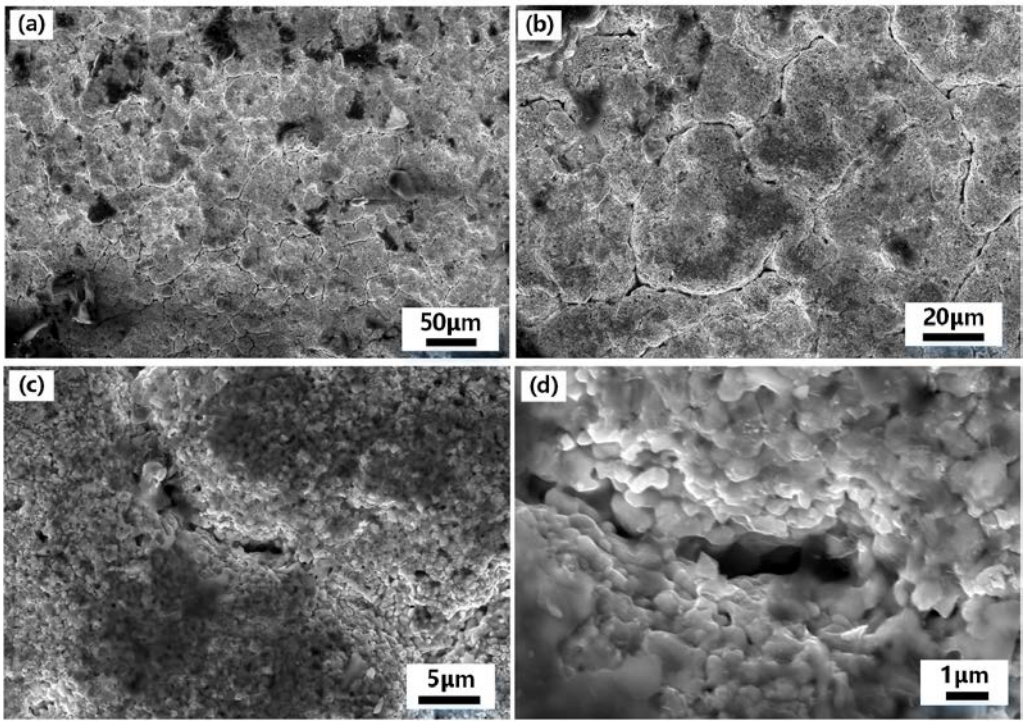

Figure 3. SEM images of the coating of the sample prepared by hot-press sintering process: (a)−(d) SEM images of the coating of the sample prepared by hot-press sintering process:(a)low-magnification view of Hf coating at 50 μm;(b)low-magnification view of Hf coating at 20 μm;(c)high-magnification view of Hf coating at 5 μm;(d)high-magnification view of Hf coating at 1 μm.

To clarify the composite mechanism between the coating prepared by the hot-press sintering process and the matrix VZrHfNbTa HEA, the samples were systematically tested and analyzed before and after sintering. Figure 4 shows the SEM photos of the cross-section of VZrHfNbTa alloy and the energy spectrum analysis. Figure 4(a) and 4(b) show the cross-section and the side of the cross-section near the edge of the VZrHfNbTa alloy prepared by hot-press sintering, respectively, the alloy layer exhibits a dense surface, indicating an excellent hot-press sintering effect. The cross-sectional energy spectrum surface scan analysis shows that the elements of zirconium, hafnium, and niobium are uniformly distributed, while vanadium and tantalum are less concentrated near the surface. Figure 5 shows the SEM, Back-Scaterred Electron（BSE）, and energy spectrum analysis of the cross-section of the Hf-coated samples prepared by hot-press sintering. As shown in Figure 5(a) and 5(b), the center of the alloy cross-section has a clear boundary with the edge, and the thickness of the central part is about 150 μm. From the energy spectral surface scan of Figure 4(c), a layer formed from metal hafnium with a thickness of approximately 120 μm was formed on the surface of the substrate VZrHfNbTa alloy. The energy spectrum analysis shows that the elements of vanadium, niobium, and tantalum have clear boundaries with the coating. Therefore, no diffusion of elements was observed during the hot pressing sintering process, and the hafnium in the coating has a distinct boundary due to its different concentration compared to the substrate alloy. In contrast, the boundary between zirconium and the coating in the cross-section is very blurred, which indicates a significant diffusion and migration of zirconium of the substrate alloy to the coating occurred during the hot-press sintering process.

Preprints (www.preprints.org) | NOT PEER-REVIEWED | Posted: 28 June 2023 doi:10.20944/preprints202306.1962.v1

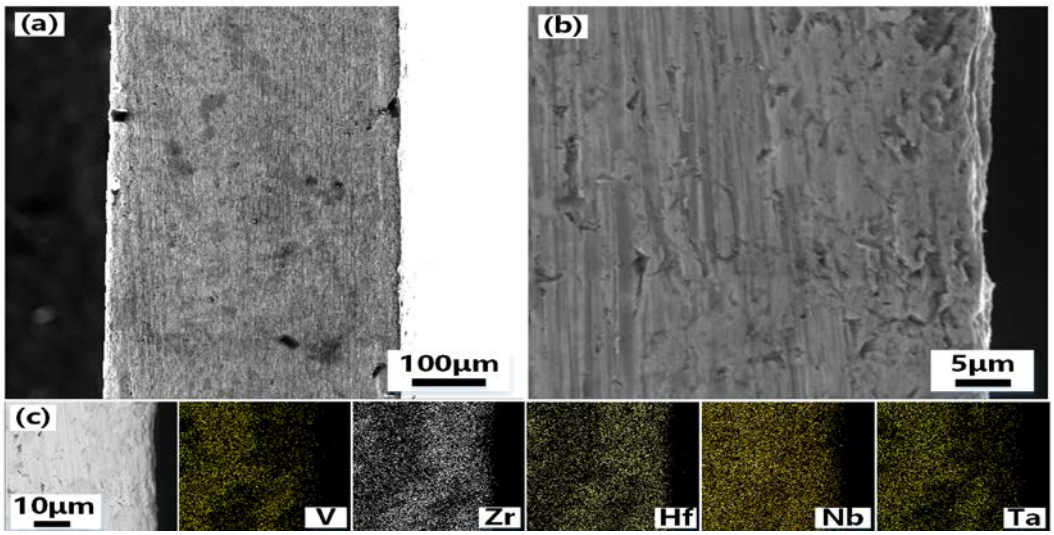

Figure 4. SEM images and EDX analysis of the cross-section of the VZrHfNbTa HEA: (a)low-magnification view of the cross-section of VZrHfNbTa high entropy alloy;(b)high-magnification view of the cross-section of the edge side of the VZrHfNbTa high entropy alloy;(c) EDX of V, Zr, Hf, Nb and Ta elements in cross sections of bulk high-entropy alloys.

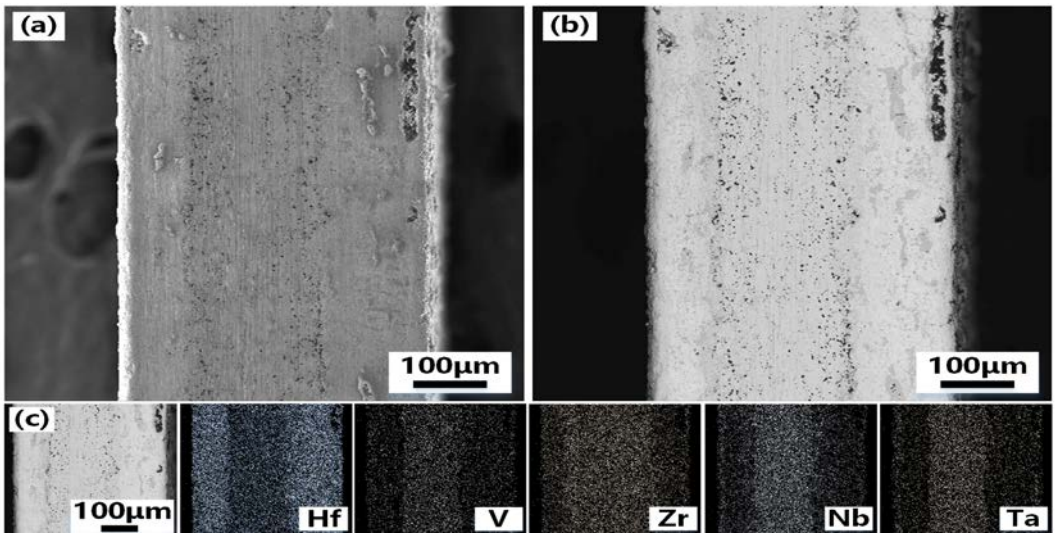

Figure 5. (a) SEM, (b) BSE images, and (c) EDX analysis of the coating sample cross-section:(a) SEM of sample cross-section of alloy substrate with Hf coating;(b)BSE of sample cross-section of alloy substrate with Hf coating;(c) EDX of V, Zr, Hf, Nb, and Ta elements in the cross-section of high entropy alloy possessing Hf coating.

To further clarify the distribution of elements at the interface between the coating and the substrate, energy spectral line scan analysis was applied to the cross-section of the coated sample. Figure 6 shows the SEM, BSE, and energy spectrum line scan analysis of a half cross-section of the hafnium-coated sample prepared by hot-press sintering. As shown in Figure 6(b), the phase difference between the substrate and the coating can be observed, but the boundary is not obvious. The white line in Figure 6(b) is the energy spectrum scan line. According to the content data of the line scan elements, the cross-section is divided into three parts: alloy matrix, HfZr coating, and hafnium coating from inside to outside. Based on the distribution of the zirconium element, it can be concluded that the diffusive distance of the zirconium element is about 60 μm when hot-press sintered at 1823 K for 1 h. the distribution of carbon element, indicate that hafnium on the coating surface and carbon paper formed hafnium coating during the hot-press sintering process, but the

Preprints (www.preprints.org) | NOT PEER-REVIEWED | Posted: 28 June 2023 doi:10.20944/preprints202306.1962.v1

thickness of HfC coating is less than 10 μm due to the limited diffusive distance of carbon element, and the carbon at the interface between the substrate and the coating mainly originates from the mixture of metal hafnium prepared by electro-deoxygenation and HfC powder in the coating, and the diffusive distance is similar to the thickness of the surface HfC. The migration of zirconium elements at the interface between the coating and the substrate helps to improve the bondability between the coating and the substrate, thus effectively improving the protection of the coating against the substrate. Figure 6(b) illustrates that a chemically bonded interface was formed in the coating, which enhances the adhesion between the coating and the substrate and solves the problem of peeling that commonly occurred in traditional alloy coating. In the VZrHfNbTa system, zirconium and hafnium belong to the same main group with similar physical and chemical properties, and Table 1 shows the basic parameters of the alloying elements. The closer the atomic radii between the alloying elements in HEAs, the more similar type of crystal structure between the group elements, the smaller the electronegativity difference, the easier it is for two infinite intercalations, then the more favorable to the formation of solid solution. According to the Miedema model [24], it is known that the enthalpy of mixing of Hf-Zr is 0, therefore, the two elements tend to form a stable solid solution. And only the zirconium and hafnium undergo the BCC→HCP isomeric transition at low temperatures as well. After the HCP solid solution is formed, there will be serious lattice distortion, which may be one of the factors that affect the diffusion of zirconium.

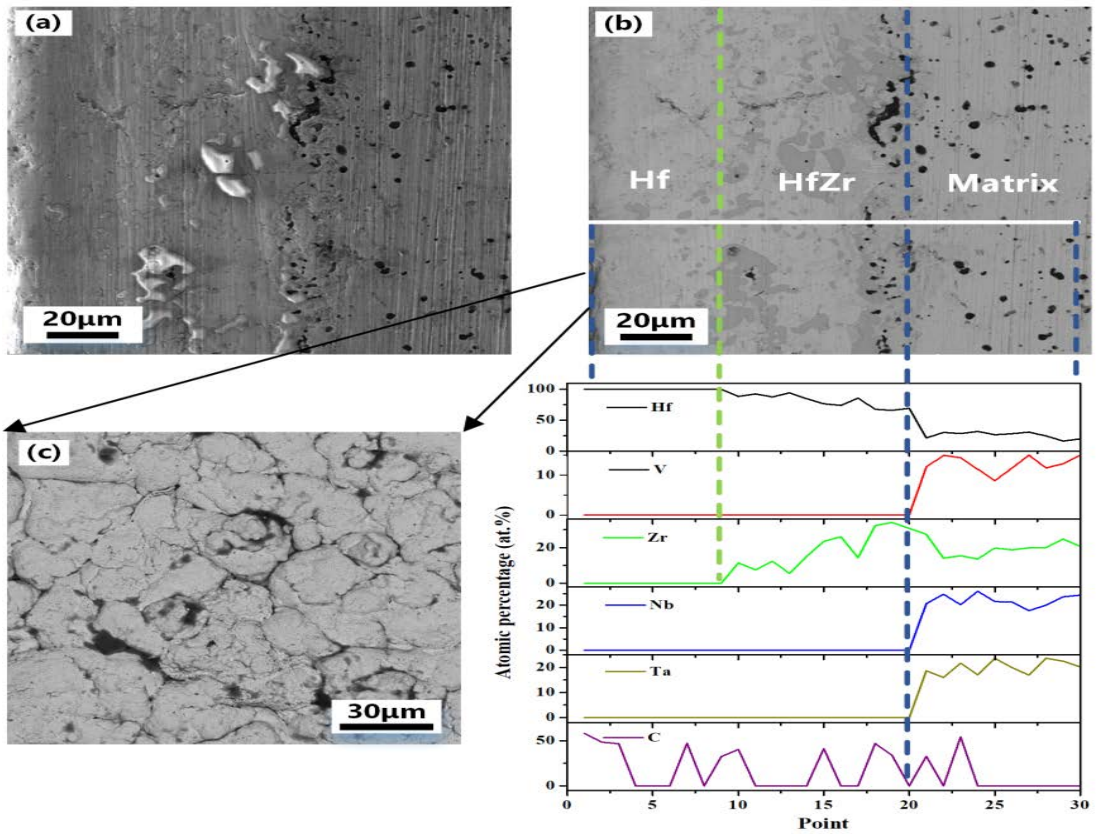

Figure 6. (a) SEM image of a cross-section of alloy sample with Hf coating. (b) BSE image and EDX image of a cross-section of alloy sample with Hf coating. (c) SEM image of Hf coating surface.

Table 1. Basic parameters of alloying elements.

Elements	V	Zr	Hf	Nb	Ta
atomic mass（g/mol）	50.94	91.22	178.49	92.91	180.9
Atomic radius（nm）	0.132	0.158	0.159	0.143	0.147
Density（g/cm^3）	5.80	6.49	13.1	8.55	16.6
Melting point（K）	2175	2125	2500	2740	3287

Preprints (www.preprints.org) | NOT PEER-REVIEWED | Posted: 28 June 2023 doi:10.20944/preprints202306.1962.v1

Boiling point（K）	3682	4682	4876	5017	5731
Crystal structure（Low Temperature）	BCC	HCP	HCP	BCC	BCC
Crystal structure（High temperature）	BCC	BCC	BCC	BCC	BCC
Crystal structure transition temperature（K）	—	1135	2033	—	—
Lattice constants（nm）	0.304	0.361	—	0.330	0.330
Electronegativity	1.63	1.33	1.3	1.6	1.5

In a certain period, Figure 7 shows the weight change curves of the specimens with and without coating during isothermal oxidation in air at a temperature of 1873 K. With the extension of oxidation time, the rate of the sample with Hf coating weight gain increased, while the rate of the sample without Hf coating weight gain slowed down. Two samples may reach an equal weight after a long enough oxidation time, but the coated sample still has better high-temperature oxidation resistance and mechanical properties. It can be seen that the weight gain per unit area of the Hf-coated alloy is significantly smaller than that of the uncoated VZrHfNbTa alloy. As shown in Figure 8, SEM comparisons of the surface of specimens with and without hafnium coating before and after oxidation. The surface SEM of the specimen before oxidation shows that the uncoated VZrHfNbTa alloy in Figure 8(a) had a dense surface, in contrast, the Hf-coated specimen in Figure 8(d) had chaps due to the sintering volume shrinkage. After oxidation for 5 h, the surface of the uncoated VZrHfNbTa alloy is shown in Figure 8(b), it illustrates obvious dents and surface pulverization, and in Figure 8(e), it can be observed that the Hf-coated specimen underwent obvious oxidation sintering, characterized by the disappearance of surface pulverization and appearance of ablation marks. The BSE photograph of the specimen surface at high magnification after oxidation is shown in Figure 8(c), the surface erosion of the uncoated VZrHfNbTa alloy is obvious and different phases were produced. And the energy spectrum analysis reveals the presence of a large amount of oxygen on the surface of the alloy. This indicates that severe oxidation occurred in the VZrHfNbTa alloy, and the different oxidation degrees of the different elements led to the pulverization of the alloy surface. The surface of the Hf-coated specimen in Figure 8(f) is dense and there is no other phase generation. The energy spectrum analysis shows that a dense HfO_2 protective layer was formed on the surface of the Hf-coated specimen after oxidation, therefore, hafnium and a minor amount of HfC in the coating were oxidized to form HfO_2 and induced a sintering reaction on the coating surface.

The specimen sections were analyzed to determine the condition of oxidation inside the two specimens. Figure 9 shows the SEM and BSE images of the coated and uncoated specimens' cross-sections after oxidation and the respective energy spectrum analyses. From the BSE photograph of the coated specimen cross-section in Figure 9(b), The phase difference between the substrate and the coating cannot be distinguished after oxidation for 5 h. The energy spectrum analyses in Figure 9(e) show that almost all elements have emerged with significant diffusion and cannot be distinguished from the boundary of the coating, except vanadium, which has a clear boundary with the coating. This is due to the significant diffusion and migration of the elements within the specimen at the high temperature of 1873 K. However, the poor compatibility of vanadium with other alloying elements resulted in the slow diffusion and migration of vanadium. The distribution of oxygen elements shows that a certain degree of oxidation occurred in the overall cross-section of the coated specimen. From the high magnification BSE image of the cross-section of the uncoated specimen in Figure 9(d), it can be seen that the interior of the alloy shows oxidation and pulverization as the same as the alloy surface. The energy spectrum analyses in Figure 9(f) show that the internal alloy experienced severe oxidation additionally, the uncoated specimen had a notably higher oxygen content compared to the coated specimen. The surface hardness of the specimens was further compared before and after oxidation, and Figure 10 shows the comparison of the surface hardness of specimens with and without hafnium coating before and after oxidation. The results indicate the surface hardness of the coated specimen decreased by 145 HV, which decreased from 1612 HV before oxidation to 1467 HV after oxidation, with a reduction of 8.995 %; the surface hardness of the uncoated VZrHfNbTa HEA

Preprints (www.preprints.org) | NOT PEER-REVIEWED | Posted: 28 June 2023 doi:10.20944/preprints202306.1962.v1

decreased by 883 HV, which decreased from 1534 HV before oxidation to 651 HV after oxidation, with a reduction of 57.562 %, and the specimen experienced significant deformation. This can be attributed to the oxidation and pulverization of the VZrHfNbTa HEA. And the hardness of the coated specimen changed less, possibly due to the HfC and hafnium in the coating forming a dense HfO_2 protective layer after oxidizing and sintering.

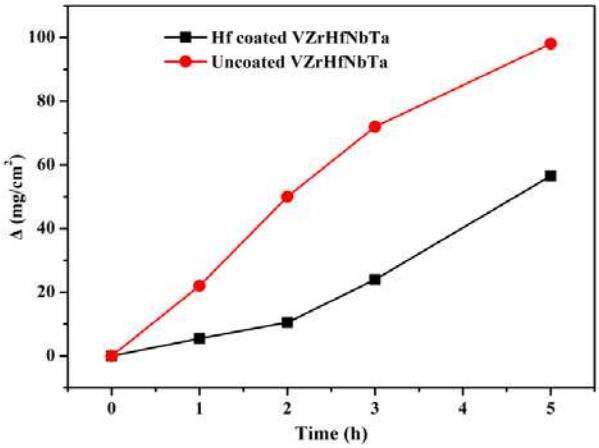

Figure 7. Weight change curves obtained for uncoated and coated VZrHfNbTa specimens during isothermal oxidation at 1873 K in air.

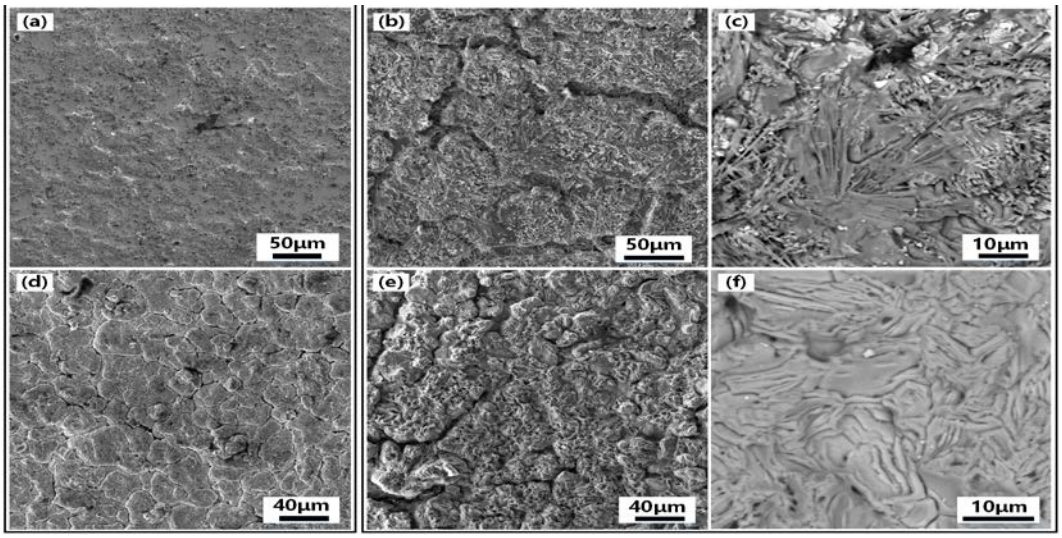

Figure 8. SEM and BSE images of uncoated specimen surface before and after oxidation and SEM and BSE images of Hf coated specimen surface before and after oxidation (a)SEM image of the surface of uncoated alloy specimen before oxidation,(b) SEM image of the surface of uncoated alloy specimen after 5 hours of oxidation,(c) high-magnification BSE image of the surface of uncoated alloy specimen after 5 hours of oxidation;, (d) – (f):,(d) SEM image of the surface of the alloy specimen with Hf coating before oxidation,(e) SEM image of the surface of the alloy specimen with Hf coating after 5 hours of oxidation,(f) High magnification BSE image of the surface of the alloy specimen with Hf coating after 5 hours of oxidation.

Preprints (www.preprints.org) | NOT PEER-REVIEWED | Posted: 28 June 2023 doi:10.20944/preprints202306.1962.v1

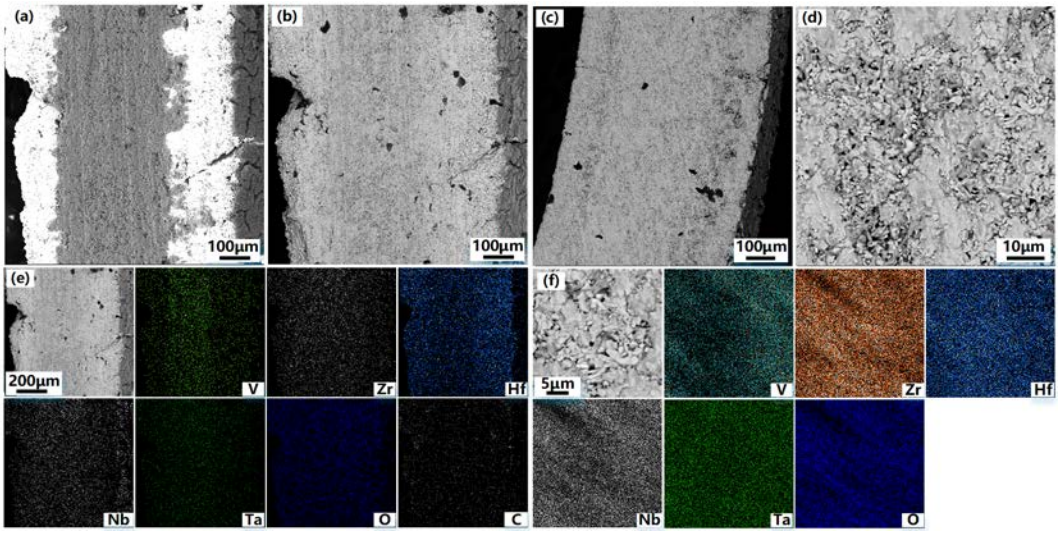

Figure 9. SEM, BSE images, and EDX analyses of the coated specimen cross-section after oxidation (a) SEM image of coated specimen sections after oxidation;(b) BSE image of coated specimen sections after oxidation; (e) EDX images of individual elements of coated specimen sections after oxidation;(c d f) SEM, BSE images and EDX analyses of the uncoated specimen cross-section after oxidation.: (c) SEM image of uncoated specimen sections after oxidation;(d) high-magnification BSE image of uncoated specimen sections after oxidation; (f) EDX images of individual elements of uncoated specimen sections after oxidation.

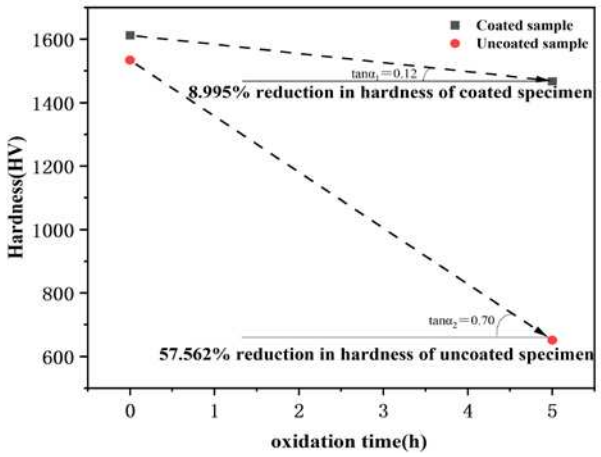

Figure 10. Comparison curves of surface hardness changes of coated and uncoated samples during air isothermal oxidation at 1873 K.

4. CONCLUSION

High-temperature oxidation-resistant VZrHfNbTa refractory HEA-based Hf-coated composites were prepared by the combined process. It has a coating thickness of 120 μm. Vanadium, niobium, tantalum and hafnium elements in the base alloy have obvious boundaries with the hafnium coating, and the zirconium element underwent diffusion and migration in the coating with a diffusive distance of about 60 μm. High-temperature oxidation tests showed that the weight gain per unit area of the coated sample was much less than that of the uncoated sample. Dents and pulverization on the surface of the alloy after oxidation of the uncoated specimen, oxidation, and sintering on the surface of the coated specimen resulted in the formation of a dense HfO_2 protective layer. The coating can effectively improve the oxidation resistance of the material in extreme environments and prevent the surface from chalking, thus extending the service life of the material and broadening the application. After oxidation, most of the elements in the coated specimen diffused significantly and the

boundaries with the coating were indistinguishable, except for the vanadium element in the coated specimen, which did not diffuse significantly and had a clear boundary with the coating. Oxidation and pulverization were observed inside the uncoated specimen, and the oxidation inside the alloy was more severe than that of the alloy matrix inside the coated specimen. The surface hardness of the uncoated specimen decreased significantly after oxidation, while the coated specimen changed less.

Funding: This work was supported by the Chongqing Natural Science Foundation (cstc2021jcyj-msxmX1049).

References

1. I, Bednarczyk, D.Kuc, G.Niewielski, The structure of FeAl and Fe3Al-5%Cr intermetallic phase-based alloys after hot deformation processes, Archives of Materials Science and Engineering,2008,30(1):5-8.
2. J.Sato, T.Omori, K.Oikawa, Cobalt-base high-temperature alloys, Science, 2006,312(5770): 90~91.
3. C.T. Sims, N.S, Stoloff, W C. Hagel, Superalloys II, United States: N. p.,1987.
4. Gui Weimin, Study on carbide evolution and related properties of cobalt-based high-temperature alloys, Ph. D. Thesis, University of Science and Technology of China,2017.
5. Nithin, B, Chattopadhyay, K. & Phanikumar, G, Characterization of the Hot Deformation Behavior and Microstructure Evolution of a New γ-γ′ Strengthened Cobalt-Based Superalloy, Metall Mater Trans A 49, 4895–4905 (2018).
6. Sato J, Omori T, Oikawa K, Cobalt-base high-temperature alloys, Science, 2006,312(5770): 90-91.
7. Qu Sasha, Tissue stability and properties of a new low-density γ'-phase strengthened cobalt-based high-temperature alloy, Ph. D. Thesis, University of Science and Technology of China,2021.
8. Pan, Yuanshui, Wang, Gang, Feng, Haixia, Effect of bonding agent type on the erosion resistance of corundum-spinel castables to nickel-based high-temperature alloys, Refractory Materials,1-9[2022-10-23].
9. J.L.Yu, Z.K.Li, X.Zheng, Tensile Properties of Multiphase Mo-Si-B Refractory Alloys at Elevated Temperatures, Materials Science & Engineering A,2011.532(3):392-395.
10. Zhu Baohui, Wu Xiangdong, Wan Min, Advances in high-temperature niobium-based alloys for aerospace applications, Chinese Journal of Nonferrous Metals.
11. Saint-Antonin F, Lefebvre W, Blum I, Nobium Base Superalloys: Achievement of a Coherent Ordered Precipitate Structure in the Nb Solid-Solution, Crystals,2019,9(7): 345.
12. Karpov M I, Niobium-base refractory alloys with silicide and carbide hardening current status and prospects, Metal Science and Heat Treatment,2018,60(1-2):7-12.
13. Nico C, Monteiro T, Graca M P F, Niobium oxides and niobates physical properties: Review and prospects, Progress in Materials Science, 2016,80: 1-37.
14. Perkins R A, Meier G H, The oxidation behavior and protection of niobium, JOM,1990,42(8): 17-21.
15. N.I. Baklanovaa, V. Victor, One-step preparation of $TaIr_3$-based material and its ablation performance under extreme environmental conditions, Corrosion Science, 2018,143(Oct.):337-346.
16. Y. Yamabe-Mitarai, H. Murakami, Mechanical properties at 2223 K and oxidation behavior of Ir alloys, Intermetallics, 48 (2014), pp. 86-92.
17. Y. Yamabe-Mitarai, H. Murakami, High-temperature oxidation resistance of Ir-based alloys, Mater. Jpn., 52 (9) (2013), pp. 440-444.
18. Senkov O N, Wilks G B, Scott J M, Mechanical properties of Nb25Mo25Ta25W25 and V20Nb20Mo20Ta20W20 refractory high entropy alloys, Intermetallics,2011,19(5):698-706.
19. Senkov, G. B. Wilks, D.B. Miracle, Refractory High-Entropy Alloys, Intermetallics, 2010,18(9):1758-1765.
20. E.Fazakas, V.Zadorzhnyy, L.K.Varga, Experimental and Theoretical Study of Ti20Zr20Hf20Nb20X20(X=V or Cr)Refractory High-entropy Alloys, International Journal of Refractory Metals & Hard Materials,2014,47(11):131-138.
21. Y.D.Wu, Y.H. Cai, T.Wang, A Refractory Hf25Nb25Ti25Zr25 High-entropy Alloy with Excellent Structural Stability and Tensile Properties, Materials Letters,2014,130(3):277-280.
22. J.P. Couzinie, L. Listen,Y.Champion, On the Room Temperature Deformation Mechanisms of a TiZrHfNbTa Refractory High-Entropy Alloy, Materials Science and Engineering a-Structural Materials Properties Microstructure and Processing,2015,645:255-263.
23. Li Chong, Design and high-temperature performance of ZrBz-based ultra-high-temperature ceramic coatings, University of Chinese Academy of Sciences (Shanghai Institute of Silicate, Chinese Academy of Sciences),2019.
24. Takeuchi A, Classification of bulk metallic glasses by atomic size difference, the heat of mixing and period of constituent elements and its application to characterization of the main alloying element, Materials Transactions,2005,46:2817-2829

 doi:10.20944/preprints202306.1962.v1

disclaim responsibility for any injury to people or property resulting from any ideas, methods, instructions or products referred to in the content.